Available online at www.sciencedirect.com

ScienceDirect

Procedia CIRP 111 (2022) 134–137

www.elsevier.com/locate/procedia

12th CIRP Conference on Photonic Technologies [LANE 2022], 4-8 September 2022, Fürth, Germany

Determination of optimum process parameters for different Ti-6Al-4V powders processed by Laser-based Powder Bed Fusion

Nicole Emminghaus[a,*], Robert Bernhard[a], Jörg Hermsdorf[a], Stefan Kaierle[a,b]

[a]*Laser Zentrum Hannover e.V., Hollerithallee 8, 30419 Hannover, Germany*
[b]*Leibniz Universität Hannover, Institut für Transport- und Automatisierungstechnik, An der Universität 2, 30823 Garbsen, Germany*

* Corresponding author. Tel.: +49-511-2788-355; fax: +49-511-2788-355. *E-mail address:* n.emminghaus@lzh.de

Abstract

The PBF-LB (laser-based powder bed fusion) process is subject to a large number of variables, including the characteristics of the processed powder. Since a powder with a given specification can be supplied by various powder manufacturers, the transferability of optimized parameter settings and statistical processing models is of major interest. This work therefore investigates the processing windows of two Ti-6Al-4V powders supplied by different manufacturers following the Design of Experiments (DoE) approach. The fitted regression models for porosity and roughness demonstrate a significant influence of the powder and its size distribution. Further, the powder type significantly interacts with laser power, scanning speed and hatch spacing. It is shown that an increase of the powder size distribution quantiles by less than 10 µm leads to a shift of optimum settings towards a higher volume energy density by 6.4 J/mm³ as well as to higher roughness on the top and side surfaces.

Keywords: Additive manufacturing; laser-based powder bed fusion; Ti-6Al-4V; Design of Experiments; roughness

1. Introduction

PBF-LB/M (laser-based powder bed fusion of metals) is a manufacturing process, in which metal powder is deposited layer by layer and melted by a laser beam according to given slicing information. Decisive for the laser material interaction and therefore the resulting part properties are the characteristics of the processed powder. These include the morphology, porosity, mean particle size and particle size distribution (PSD) as well as the chemical composition. They determine the flow and spreading behavior as well as the laser absorption and melting process. However, powder properties are subject to variations. These are mainly due to fluctuations between production batches, recycling and ageing. In addition, powders from different manufacturers can differ from each other although specified identically. As a result, problems arise when the powder supplier has to be changed because of delivery bottlenecks or portfolio changes.

The change of powder properties and resulting influences on the process have been reported in the literature. A wider PSD generally leads to a higher packing density and a decreased flowability while with increasing mean particle size the flowability increases [1,2]. A higher flowability and packing density in turn leads to higher part density [3]. Regarding the influence of powder properties on mechanical properties, contradictory results are reported in the literature. While Seyda et al. did not observe significant differences for three different Ti-6Al-4V powders [4], Liu et al. reported an increase of hardness for a narrower PSD of 316L powder [5]. For different batches of Ti-6Al-4V powder, Soltani-Tehrani et al. noticed small differences in roughness and microstructure [6].

A common approach to investigate differences between different powder batches is to process both of them with the same parameter set. However, this approach provides insufficient information on how existing parameter sets need to be adjusted, when a different powder, e.g. from another powder

10.1016/j.procir.2022.08.052

supplier or a recycled powder batch, should be processed. Hence, it is necessary to conduct a multivariate parameter study for the different types of powder, which is a novelty to the current state of the literature. Building on this, inferences on the transferability of the processing window can be made. This work therefore focusses on the development of empirical process models using the design of experiments approach and statistical regression analysis.

2. Materials and Methods

2.1. Experimental Design and Equipment

In this work, two Ti-6Al-4V powder batches from different suppliers were investigated. Prior to processing, the powder was characterized according to DIN EN ISO 3923 and 4490. Additionally the PSD was determined using image analysis consisting of segmentation and edge detection in ImageJ. The characterization results and additional information from the suppliers' inspection certificates are displayed in Table 1 and 2. Fig. 1 shows the SEM images of the investigated powders. To investigate the influence of different powder batches and their properties on the porosity and roughness of the manufactured parts, a central composite design (CCD) was applied. The parameters laser power, scanning speed and hatch spacing were varied on five levels each according to this design. This was repeated for two different layer thicknesses (30 µm and 50 µm) and for both powder batches resulting in four build jobs. All parameter combinations were repeated three times per build job except the center point, which was repeated six times leading to 48 specimens per build job. Table 3 gives an overview of the applied parameter settings. The experiments were conducted on an industrial machine (Lasertec 12 SLM by DMG MORI) that is equipped with a 400 W fiber laser (1070 nm, continuous wave, minimum spot diameter of 35 µm).

Table 1. Results of powder characterization.

Characteristic	Powder A	Powder B
Supplier	Heraeus Additive Manufacturing GmbH	ECKART TLS GmbH
Specified size	15 – 53 µm	20 – 53 µm
D10 (laser diffraction, by supplier)	21.65 µm	28.82 µm
D50 (laser diffraction, by supplier)	36.62 µm	41.75 µm
D90 (laser diffraction, by supplier)	53.17 µm	60.31 µm
D10 (image analysis)	8.60 µm	9.43 µm
D50 (image analysis)	19.04 µm	26.87 µm
D90 (image analysis)	36.69 µm	47.43 µm
Flow rate (s/50 g) (by supplier)	-	33,69
Flow rate (s/50 g) (Hall)	-	38
Flow rate (s/50 g) (Carney)	16	7
Apparent density (g/cm³) (by supplier)	2.51	2.25
Apparent density (g/cm³) (Hall)	-	2.23
Apparent density (g/cm³) (Carney)	2.46	2.24

Table 2. Chemical composition of the powder batches derived from the suppliers' inspection certificates.

Element (wt.%)	Ti	Al	V	O	Fe	N
Powder A	balance	6.03	3.86	0.105	0.15	0.018
Powder B	balance	6.21	3.98	0.07	0.199	0.009

Table 3. Implemented factor levels.

Parameter	Factor levels				
Laser power P (W)	115	145	175	205	235
Scanning speed v (mm/s)	600	800	1000	1200	1400
Hatch spacing h (µm)	40	60	80	100	120
Layer thickness t (µm)	30			50	
Powder	A			B	

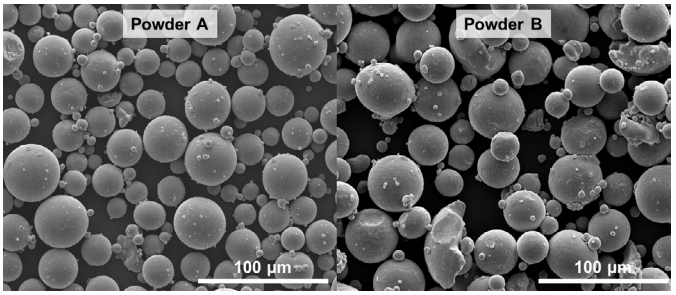

Fig. 1. SEM images of the investigated powders.

2.2. Methods for Analysis

For each parameter combination, one specimen was evaluated using optical profilometry (laser scanning confocal microscope VK-X1000 by Keyence). The roughness metric S_a was determined for the top and the side surfaces for an 1 mm · 1 mm area. In a next step all specimens were cold embedded, ground and polished. By using light microscopy, the mean porosity for three cross-sections per specimen was determined.

Based on the results for roughness and porosity, regression models were fitted using the least squares method. The porosity response was log-transformed to reduce heteroscedasticity. A significance level of 5 % (p-value = 0.05) was chosen and all effects with larger p-values were excluded from the model while following the principle of strong effect heredity. The statistical analysis was conducted using the statistics software JMP® (SAS Institute Inc.). Since the prediction variance outside of the corner points of the CCD is poor, optimum settings for all responses were determined only within the corner points of the varied factors.

3. Results

3.1. Roughness

The roughness measurements showed that in general the side surfaces exhibit a higher roughness than the top surfaces. The top surfaces exhibit a structure dependent on the scanning direction (SD). This is also visible in Fig 2.

For the top surface a minimum of S_a = 6.234 µm (Powder A, P = 175 W, v = 600 mm/s, h = 80 µm, t = 30 µm) and a maximum of S_a = 17.737 µm (Powder B, P = 145 W, v = 1200 mm/s, h = 100 µm, t = 30 µm) were obtained. For the side surface the minimum was S_a = 7.37 µm (Powder A, P = 205 W, v = 800 mm/s, h = 100 µm, t = 50 µm) and the maximum was S_a = 24.976 µm (Powder B, P = 175 W, v = 600 mm/s, h = 80 µm, t = 50 µm).

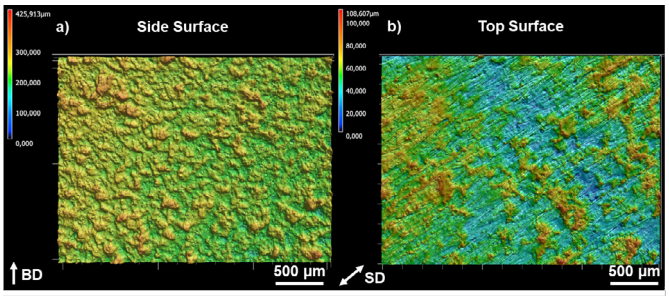

Fig. 2. Surface topology of manufactured samples, a) side surface, b) top surface (central point, powder B), arrows indicate build and scan direction (BD, SD).

In general, powder B with a larger mean particle size leads to higher roughness on both surfaces. Additionally, the top surface roughness decreases and the side surface roughness increases with increasing volume energy density E_V that is calculated as follows:

$$E_V = \frac{P}{v \cdot h \cdot t} \quad (1)$$

The parameter estimates of the regression models (Appendix A.1 and A.2) show, that all varied factors had a significant influence. While the top surface was mostly influenced by the scanning speed, the side surface roughness was mostly influenced by the interaction effect of scanning speed and hatch spacing followed by the powder material.

3.2. Porosity

A minimum porosity of 0.007 % (Powder A, P = 175 W, v = 1000 mm/s, h = 120 µm, t = 30 µm) could be obtained. The maximum porosity was 4.014 % (Powder B, P = 145 W, v = 1200 mm/s, h = 100 µm, t = 50 µm). The largest effect regarding the regression model for the porosity is the interaction effect of laser power and scanning speed (Appendix A.3). Laser power, scanning speed and hatch distance show significant quadratic effects and interactions. Consequently, there is an optimum setting for minimum porosity within the investigated parameter range. Above the resulting optimum E_V, the applied energy is too high causing overheating and gas pores. Below, the energy input is insufficient to melt the powder completely and lack-of-fusion porosity can be observed.

3.3. Optimal settings and transferability

Based on the regression models that are given by the parameter estimates in the appendix, the optimal parameter settings for minimal roughness and porosity were determined (see Table 7).

Table 7. Optimal parameter settings.

Response	Powder	P (W)	v (mm/s)	h (µm)	t (µm)	E_V (J/mm³)
Porosity	A	165	945	100	30	58.2
	B	175	950	95	30	64.6
Top surface roughness	A	170	800	100	30	70.8
	B	180	800	100	30	75.0
Side surface roughness	A	205	800	100	30	85.4
	B	205	830	100	30	82.3

It can be seen that in order to achieve minimum porosity an increase of E_V by 6.4 J/mm³ is necessary. More precisely, especially an increase of the laser power by 10 W is needed in regard of the porosity as well as the top surface roughness. For the side surface roughness, less significant changes of the parameter settings are needed since this response variable mainly depends on the used powder itself.

4. Discussion

With regard to the roughness results obtained, different roughness mechanisms for the top and side surfaces can be identified: The top surface roughness is mainly formed by the balling effect because of insufficient melting and adhering spatter particles. With higher energy input and decreasing melt viscosity the improved melt spreading reduces the surface roughness [7,8]. A larger mean particle size in turn requires a higher melting energy and additionally leads to larger spattered particles. On side surfaces, the main roughness mechanism are adhering, partly melted particles. The higher the energy input the more the melt infiltrates the surrounding powder leading to an increase of the side surface roughness. Additionally, the roughness directly depends on the size of the adhering particles and therefore on the powder PSD.

Since the porosity is mainly influenced by the laser process parameters (P, v, h), changes in the powder can be counteracted by adjusting these parameters. In this way, a minimum porosity of less than 0.02 % can still be achieved.

5. Conclusion

In this work, the transferability of process parameters using different Ti-6Al-4V powder batches was investigated. The following conclusions can be given based on the determined parameter estimates of the regression models (see appendix):

- The roughness on the top and side surface is significantly influenced by the used powder and its mean particle size. Different roughness mechanisms apply to the different types of surfaces.
- The porosity is mainly influenced by the laser process parameters. There are significant interaction effects of these parameters with the used powder since larger particles require a higher energy input for sufficient melting.

- Transferability investigations require the application of multivariate parameter studies to find optimum parameter settings. While a minimum porosity and top surface roughness can be maintained by parameter adjustment, the side surface roughness is forced to change when the PSD is changed.

This study stresses that every powder needs thorough characterization to ensure a consistent quality and applicability of parameter settings. Future work will concentrate on the transferability between different recycling grades and machine setups.

Acknowledgements

Funded by the Deutsche Forschungsgemeinschaft (DFG, German Research Foundation) – Project-ID 394563137 – SFB 1368.

Appendix A. Regression models - Parameter estimates and p-values

A.1. Top surface roughness S_a in µm

Term	Estimate	Std. Error	t-Ratio	p-Value
Intercept	3.0778	1.2909	2.38	0.0213
Scanning speed	2.5360	0.5507	4.61	<0.0001
Laser power · Scanning speed	-1.3473	0.4007	-3.36	0.0016
Scanning speed · Hatch spacing	1.3123	0.4007	3.28	0.0020
Powder material [B]	1.1384	0.2926	3.89	0.0003
Laser power	-0.9778	0.5507	-1.78	0.0824
Hatch spacing	0.9040	0.2833	3.19	0.0026
Laser power^2	0.8756	0.2576	3.40	0.0014
Scanning speed^2	0.6863	0.2576	2.66	0.0106
Powder material [B] · Laser power	-0.6645	0.2833	-2.35	0.0234
Scanning speed^3	-0.6570	0.1889	-3.48	0.0011
Laser power^3	-0.4520	0.1889	-2.39	0.0208
Layer thickness	0.1713	0.0293	5.85	<0.0001
Scanning speed · (Layer thickness – 40 µm)	-0.0657	0.0283	-2.32	0.0249

A.2. Side surface roughness S_a in µm

Term	Estimate	Std. Error	t-Ratio	p-Value
Intercept	12.1208	1.1773	10.30	<0.0001
Scanning speed · Hatch spacing	1.9383	0.3827	5.06	<0.0001
Powder material [B]	1.8639	0.2795	6.67	<0.0001
Hatch spacing	-1.4185	0.2706	-5.24	<0.0001
Laser power · Scanning speed	0.9935	0.3827	2.60	0.0124
Scanning speed^2	0.9360	0.2260	4.14	0.0001
Powder material [B] · Scanning speed	-0.7732	0.2706	-2.86	0.0063
Scanning speed^3	-0.4989	0.1804	-2.77	0.0080
Scanning speed	0.3239	0.5260	0.62	0.5409
Laser power	0.1807	0.2706	0.67	0.5074
Layer thickness	0.0574	0.0280	2.06	0.0452

A.3. Log (Porosity in %)

Term	Estimate	Std. Error	t-Ratio	p-Value
Intercept	-5.1704	0.1856	-27.86	<0.0001
Laser power · Scanning speed	-0.8679	0.0547	-15.86	<0.0001
Scanning speed^2	0.6250	0.0387	16.15	<0.0001
Scanning speed · Hatch spacing	0.5237	0.0547	9.57	<0.0001
Laser power^2	0.4793	0.0387	12.39	<0.0001
Laser power · Hatch spacing	-0.3643	0.0547	-6.66	<0.0001
Hatch spacing^2	0.3251	0.0387	8.40	<0.0001
Scanning speed^3	-0.2726	0.0258	-10.57	<0.0001
Powder material [B] · Scanning speed	0.2064	0.0387	5.33	<0.0001
Powder material [B] · Laser power	-0.2057	0.0387	-5.32	<0.0001
Powder material [B]	0.1728	0.0387	4.47	<0.0001
Scanning speed	0.1662	0.0752	2.21	0.0285
Hatch spacing	-0.1647	0.0752	-2.19	0.0299
Laser power^3	-0.1139	0.0258	-4.41	<0.0001
Powder material [B] · Hatch spacing	0.1064	0.0387	2.75	0.0066
Hatch spacing^3	-0.0584	0.0258	-2.26	0.0249
Laser power	0.0347	0.0752	0.46	0.6455
Scanning speed · (Layer thickness – 40 µm)	0.0319	0.0039	8.23	<0.0001
Laser power · (Layer thickness – 40 µm)	-0.0312	0.0039	-8.06	<0.0001
Layer thickness	0.0302	0.0039	7.81	<0.0001
Hatch spacing · (Layer spacing – 40 µm)	0.0221	0.0039	5.71	<0.0001

References

[1] S.E. Brika, M. Letenneur, C.A. Dion, V. Brailovski, Influence of particle morphology and size distribution on the powder flowability and laser powder bed fusion manufacturability of Ti-6Al-4V alloy, Additive Manufacturing 31 (2020) 100929.

[2] M. Habibnejad-Korayem, J. Zhang, Y. Zou, Effect of particle size distribution on the flowability of plasma atomized Ti-6Al-4V powders, Powder Technology 392 (2021) 536–543.

[3] R. Baitimerov, P. Lykov, D. Zherebtsov, L. Radionova, A. Shultc, K.G. Prashanth, Influence of Powder Characteristics on Processability of AlSi12 Alloy Fabricated by Selective Laser Melting, Materials 11 (2018) 742.

[4] V. Seyda, D. Herzog, C. Emmelmann, Relationship between powder characteristics and part properties in laser beam melting of Ti–6Al–4V, and implications on quality, Journal of Laser Applications 29 (2017) 22311.

[5] B. Liu, R. Wildman, C. Tuck, I. Ashcroft, R. Hague, Investigation the effect of particle size distribution on processing parameters optimisation in selective laser melting process, Additive manufacturing research group, Loughborough University (2011) 227–238.

[6] A. Soltani-Tehrani, M. Habibnejad-korayem, S. Shao, M. Haghshenas, N. Shamsaei, Ti-6Al-4V powder characteristics in laser powder bed fusion: The effect on tensile and fatigue behavior, Additive Manufacturing 51 (2022) 102584.

[7] S. Pal, G. Lojen, R. Hudak, V. Rajtukova, T. Brajlih, V. Kokol, I. Drstvenšek, As-fabricated surface morphologies of Ti-6Al-4V samples fabricated by different laser processing parameters in selective laser melting, Additive Manufacturing 33 (2020) 101147.

[8] M. Khorasani, A. Ghasemi, U.S. Awan, E. Hadavi, M. Leary, M. Brandt, G. Littlefair, W. O'Neil, I. Gibson, A study on surface morphology and tension in laser powder bed fusion of Ti-6Al-4V, Int J Adv Manuf Technol 111 (2020) 2891–2909.